SCIENCE CHINA
Technological Sciences

July 2013 Vol.56 No.7: 1657–1666
doi: 10.1007/s11431-013-5259-5

Numerical simulation on heat transfer inside rotating porous disk subjected to local heat flux

ZHU XingDan, ZHANG JingZhou* & TAN XiaoMing

College of Energy and Power Engineering, Nanjing University of Aeronautics and Astronautics, Nanjing 210016, China

Received February 4, 2013; accepted May 13, 2013; published online May 27, 2013

Numerical simulation was carried out to study the centrifugally-driven flow and heat transfer inside rotating metallic porous disk subjected to local heat flux. The effects of rotational speed, solid thermal conductivity and porosity on heat transfer were analyzed. The thermal transport coefficient, defined as the ratio of local heat flux to maximum temperature difference on the disk, was introduced to evaluate the thermal transport capacity in rotating porous disk. For convenience, the conjugation between convective heat transfer inside the rotating porous disk and convective heat transfer over the rotating disk surface was decoupled in the present study. Firstly, the convective heat transfer over the free rotating disk surface was investigated individually to determine the heat transfer coefficient over the disk surface to the ambient air. Then the convective heat transfer over a rotating disk surface was treated as the thermal boundary condition for the computation of convective heat transfer inside rotating porous disk. Under the present research conditions, the results show that the centrifugally-driven flow is enhanced significantly with the increase of rotational speed. Consequently, the maximum temperature on the disk surface is decreased and the temperature distribution tends to be uniform. The thermal transport capacity in rotating porous disk is also enhanced with the increase of solid thermal conductivity or the decrease of solid porosity. In the rotating porous disk, the solid phase heat transfer is clearly the dominant mode of heat transport and the fluid phase makes an incremental contribution to the total heat transfer.

local heat flux, rotating disk, porous medium, centrifugally-driven flow, numerical simulation

Citation: Zhu X D, Zhang J Z, Tan X M. Numerical simulation on heat transfer inside rotating porous disk subjected to local heat flux. Sci China Tech Sci, 2013, 56: 1657–1666, doi: 10.1007/s11431-013-5259-5

1 Introduction

The grinding process requires higher energy expenditure per unit volume of material removed. Virtually all of this energy is dissipated as the heat in the grinding zone where the wheel interacts with the workpiece. The heat generated in the grinding zone is then transferred to workpiece (Q_w), grinding swarf (Q_{sf}), coolant (Q_{co}) and grinding wheel (Q_{gw}), as seen in Figure 1 [1]. As a consequence, a high temperature may be experienced by the grinding surface, which can cause various types of thermal damage, such as burning, metallurgical phase transformations, softening of hardened surfaces, unfavorable residual tensile stresses, cracks and oxidation. The traditional method for the cooling of the grinding zone uses liquid coolants, such as oil-in-water emulsion and neat oil, owing to that the liquid coolants can provide bulk cooling of the workpiece and removal of swarf [2, 3]. Substantially, environmental and resource problems have urged the search for alternative cooling agents without or with less chemical additives, which has become an active study. Numerous investigations focused on the spray and mist cooling methods [4–9]. The key problem is how to make the coolants with low speed and kinetic energy pene-

*Corresponding author (email: zhangjz@nuaa.edu.cn)

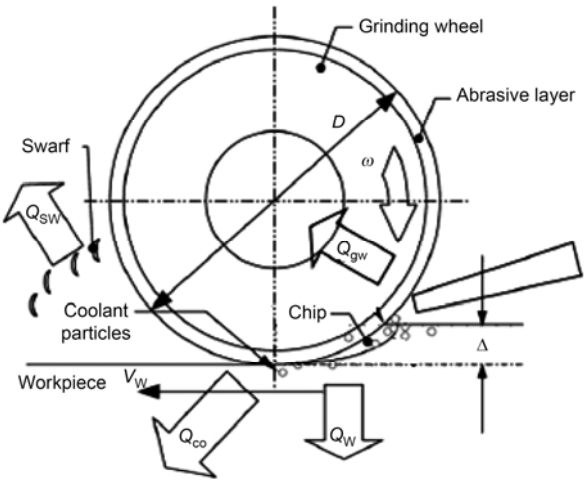

Figure 1 Schematic of grinding energy transfer.

trate the boundary layer forming around a fast-rotating grinding wheel, ensuring that they can reach good heat transfer in the grinding zone.

It is noticed that the heat generated in the vicinity of the grinding zone is mainly removed by the coolant for the existing cooling methods. Little attention has been paid to the enhancement of heat transfer from the rotating grinding wheel to the ambient surrounding. Recently, Su et al. [10] put forward a new conception of using heat pipe to enhance heat transfer in the grinding zone. A new type of grinding wheel named the loop-heat pipe wheel was developed for greatly increasing the critical heat flux. In the current study, a novel heat transfer enhancement by the rotating grinding wheel is presented. That is, the solid grinding wheel with low thermal conductivity is replaced by the metallic porous grinding wheel filled with saturated fluid. Principally, the heat generated in the vicinity of the grinding zone could be transferred strongly inside the grinding wheel basing on the centrifugally-driven flow mechanism, and then transferred from the grinding wheel surfaces to the ambient surrounding.

Using porous media to enhance heat transfer is an enduring theme in the field of thermal fluid science because of many unique advantages, such as low relative density, high surface area per unit volume, high solid thermal conductivity, and good flow-mixing capability. Especially with the development of co-sintering technique, the consolidated porous medium made of metal, particularly the metallic porous medium, gradually exhibits excellent thermal performance. In the last two decades, there have been continuous concerns on the flow and heat transfer properties of metallic foam [11−19]. Thermal convection in rotating porous media has also been investigated by many researchers [20−24]. All the work, however, is distinctly different from the current work in terms of geometry orientation and boundary conditions. To the best of our knowledge, no literature is available on the thermal transport in a rotating porous disk subjected to local heat flux at disk rim, simulating the grinding process. In the current study, numerical investigation is conducted to illustrate some of the flow and heat transfer characteristics inside rotating porous metallic disk subjected to local heat flux. The effects of rotational speed, thermal conductivity and porosity of solid matrix on heat transfer inside the rotating porous disk were analyzed. And the thermal transport coefficient, defined as the ratio of local heat flux to maximum temperature difference on the disk, was introduced to evaluate the thermal transport capacity in rotating porous disk.

2 Mathematical modeling and solution

The problem considered in the present is illustrated schematically in Figure 2. The disk with width (H) of 50 mm and radius (R) of 100 mm represents a 'fictitious' grinding wheel. It rotates with a constant angular velocity (ω) around the z-axis which is normal to the disk surface. This rotating disk is made of porous metallic foam and bounded by the impermeable thin layers (0.1 mm) with heat conductivity of 100 W/(m K). On the sectional arc located at disk rim ($\Delta\theta$=5°), a local uniform heat flux is imposed to simulate the local heating in the grinding zone. The other surfaces of the disk are treated as convective heat transfer surfaces surrounded by ambient air.

In the modeling of centrifugally-driven convective heat transfer in metallic foams, three assumptions are made for the analytical simplification. Firstly, the metallic foams are assumed to be homogeneous and isotropically saturated. Secondly, the thermal radiation is neglected and the local thermal equilibrium (LTE) assumption between the solid and fluid phases in the foam is invoked. The reason for the use of the LTE model in the current study is that it is very difficult to determine the solid-fluid interfacial heat transfer coefficient inside rotational porous medium, while for the forced convective heat transfer this interfacial heat transfer coefficient could be estimated according to the modified

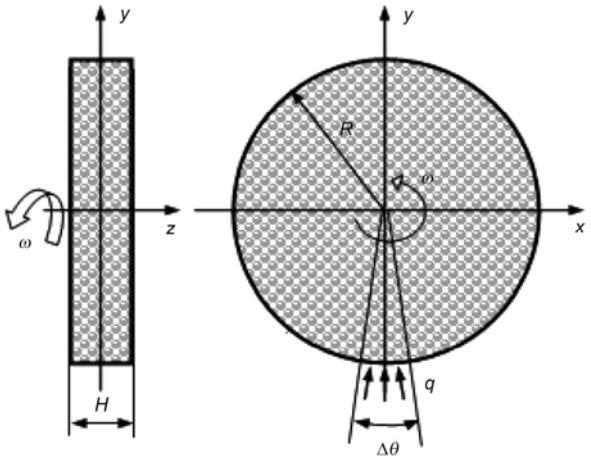

Figure 2 Schematic of physical model of rotating porous disk subjected to local heat flux.

correlations for flow over a porous channel. It is generally known that the local thermal non-equilibrium model (LTNE model) is more accurate than the LTE model where a substantial temperature difference exists between the solid phase and the fluid phase [25, 26]. However, several studies on the validity of the LTE assumption point out that the thermal equilibrium assumption is justifiable when the solid conduction is the dominant heat transfer mode (Kim and Jang [27]), or the solid-fluid interfacial heat transfer rate is very great (Chen et al. [19]). In fact, this simplification can be taken for granted in the case of thermal transport inside rotating metallic porous disk in which the solid-fluid interfacial heat transfer rate could be approximately assumed as "very great" owing to strong centrifugally-driven convective heat transfer. The third assumption is that the effective properties of the porous medium are regarded as constant. The saturated fluid inside the solid matrix is specified as hydrogen, thus no phase-change occurs inside the porous medium.).

Basically, for porous media analysis, a macroscopic form of the governing equations is obtained by taking the volumetric average of the entire equation set. Under the above approximation, the governing equations for the steady thermal transport in a fluid saturated rotating porous medium are set as follows [28]:

$$\nabla \cdot \boldsymbol{V} = 0 \tag{1}$$

$$\rho\left[\frac{1}{\phi^2}(\boldsymbol{V}\cdot\nabla)\boldsymbol{V}+\frac{2}{\phi}\boldsymbol{\omega}\times\boldsymbol{V}+\boldsymbol{\omega}\times(\boldsymbol{\omega}\times\boldsymbol{X})\right]$$
$$=-\nabla p+(\mu+\mu_{\mathrm{t}})\nabla^2\boldsymbol{V}-\frac{\mu}{K}\boldsymbol{V}+\rho\boldsymbol{g}, \tag{2}$$

$$\rho c_{\mathrm{p}}\boldsymbol{V}\cdot\nabla T=\nabla\cdot\left((\lambda_{\mathrm{e}}+\lambda_{\mathrm{t}})\nabla T\right)+\frac{\mu}{K}\boldsymbol{V}\cdot\boldsymbol{V}, \tag{3}$$

$$\rho=\rho_{\mathrm{ref}}[1-\beta(T-T_{\mathrm{ref}})]. \tag{4}$$

In comparison with the governing equations without considering rotational effect, extra body-force term is added to the momentum equation, reflecting the centrifugal and Coriolis effects. The last term in the energy equation is the viscous dissipation term, given by the power of the drag force.

In the above equations, $\boldsymbol{V}$ is the flow velocity vector, $\boldsymbol{\omega}$ is the angular velocity of the rotating frame of reference and $\boldsymbol{X}$ is the position vector relative to the frame, $\boldsymbol{g}$ is the gravitational acceleration vector. ϕ and K represent the porosity and permeability of the porous medium, respectively. p is the flow pressure and T is flow temperature. ρ, c_{p}, μ and β are the density, specific heat, viscosity and thermal expansion coefficient of the fluid, respectively. ρ_{ref} and T_{ref} are reference density and temperature, respectively. The effective conductivity of porous medium (λ_{e}) is volume average of fluid (λ_{f}) and solid (λ_{s}) medium conductivities:

$$\lambda_{\mathrm{e}}=\phi\lambda_{\mathrm{f}}+(1-\phi)\lambda_{\mathrm{s}}. \tag{5}$$

In the present study, the porosity and conductivity of the porous metallic foam are chosen as variables. And the relationship between the porosity and permeability of the porous medium is set as [19]

$$K=\frac{d_{\mathrm{p}}^2\phi^3}{144(1-\phi)^2}, \tag{6}$$

where d_{p} is the equivalent spherical diameter of a porous medium, which is taken as 5×10^{-3}m.

The macroscopic turbulent viscosity (μ_{t}) is determined from RKG k-ε turbulent model.

The porous disk is set as the computational region, as seen in Figure 3(a). The computational meshes are non-uniform with fine grids in the regions where the great velocity and temperature gradients occur, especially near the viscous walls. Nine layers are arranged near the disk wall, and first layer is set at z=0.1 mm. Then the grids are stretched away from the viscous wall using a stretching ratio of 1.1. Approximately 1500000 computational grids are involved in the computational region. The local grid dividing is shown in Figure 3(b).

For convenience, the conjugation between convective heat transfer inside the rotating porous disk and convective heat transfer over the rotating disk surface is decoupled in the present study. Firstly, the convective heat transfer over the rotating disk surface with uniform heat flux is investigated individually to determine the heat transfer coefficient over the disk surface to the ambient air. Then the convective

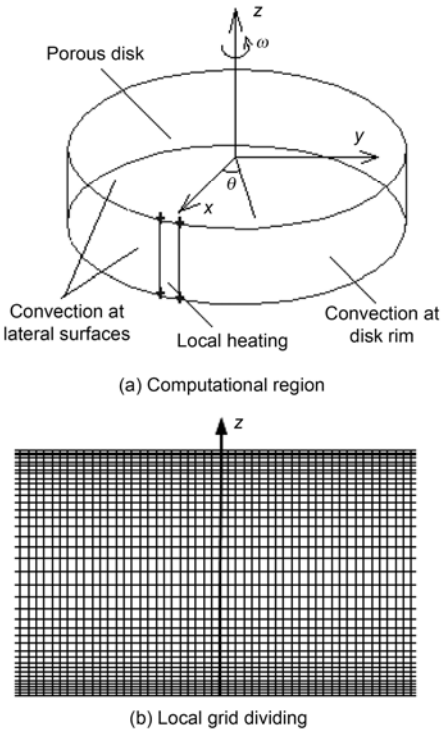

Figure 3 Schematic of computational domain and meshes.

heat transfer over a rotating disk surface is treated as the thermal boundary condition for the computation of convective heat transfer inside rotating porous disk. Therefore, the boundary conditions for the calculation of convective heat transfer inside rotating porous disk are summarized as the following:

(i) On the sectional arc located at the disk rim ($\Delta\theta$=5°), a uniform heat flux is set as q=5×10^5 W m^{-2}.

(ii) All the surfaces of the rotating disk are treated as impermeable. No-slip wall boundary conditions are imposed on all the solid surfaces.

(iii) On the other surfaces of the disk, the third thermal conditions are imposed with ambient temperature of 300 K. The convective heat transfer coefficients over the rotating disk surfaces are determined according to the next section.

The computation is carried out by using the commercial CFD software FLUENT. The simulation uses the segregated solver, which employs an implicit pressure-correction scheme and decouples the momentum and energy equations. The SIMPLE algorithm is used to couple the pressure and velocity. Second order upwind scheme is selected for spatial discretization of the convective terms. The additional body-force terms in the momentum equation and viscous dissipation term in the energy equation are introduced through the user definition function (UDF). It is necessary to control the speed of calculation by under-relaxation. Convergence is considered achieved when the following criteria have been met: reduction in all residuals of five orders of magnitude. More details on these solvers could be found in the ANSYS Fluent Software User's Guide [29].

3 Convective heat transfer on disk surface

A schematic of the physical model is shown in Figure 4, referring to a solid disk spinning at an angular speed of ω. The bottom surface of the rotating disk is subjected to a constant heat flux while the top and rim surfaces are surrounded with ambient air. This heat transfer process may be viewed as "conjugate" problem. The heat is transferred firstly from the bottom surface to the top and rim surfaces through the conduction and then transferred out from these surfaces to ambient surrounding. In the current study, the thermal conductivity of the rotating disk is set as 30 W m^{-1} K^{-1}). The radius of the rotating disk (R) is 100 mm and thickness (s) is 25 mm. The heat flux on the bottom surface is assumed uniform with q=5000 W m^{-2}. The rotating angular speed is fixed at a certain range from 500 to 3000 r min^{-1}.

The computation domain is composed of rotating disk and surrounding fluid. The fluid region is chosen as 4 times of disk diameter in radial direction and 8 times of disk thickness in axial direction. The computational grids are divided by the non-uniform meshes with fine grids near the viscous walls. Approximately 1000000 computational grids

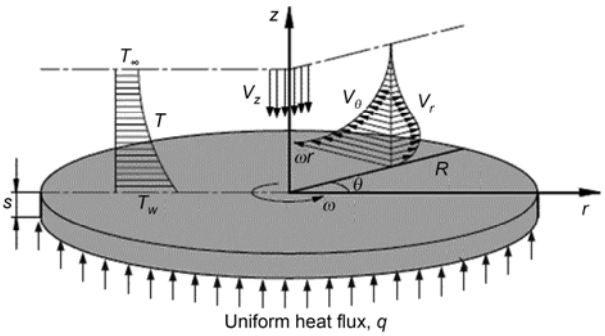

Figure 4 Schematic of free rotating disk with bottom subjected to heat flux.

are involved in the whole computational domain.

The local heat transfer coefficient (h) is defined as

$$h = \frac{q_{\text{surface}}}{T_{\text{surface}} - T_\infty}, \tag{7}$$

here q_{surface} and T_{surface} are the local heat flux and local temperature on the top of rotating disk, respectively. They are different from the corresponding values at the bottom and therefore determined by the computation. T_∞ is the ambient temperature.

The convective heat transfer on the rotating disk surface is also measured by experiment. The schematic of the experimental apparatus is illustrated in Figure 5. The rotating disk is fixed straightly on the vertical shaft which is driven to rotate by a 2000 W DC motor through the V-belt. The rotating speed can be adjusted in the range from 100 to 5000 r min^{-1}.

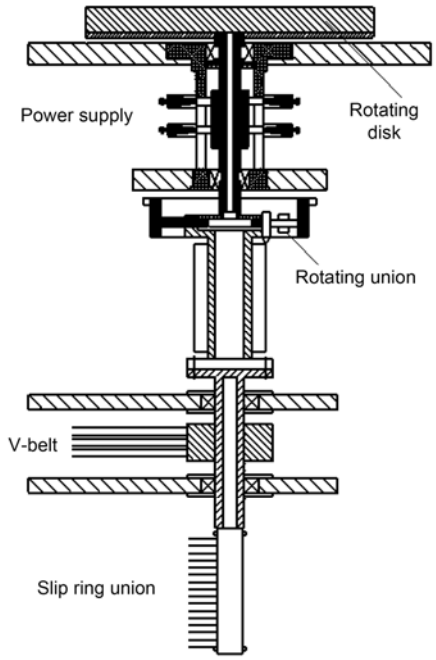

Figure 5 Schematic of the experimental apparatus.

The rotating disk is made of carbon steel (thermal conductivity is about 30 W m^{-1} K^{-1} with 25 mm in thickness and 200 mm in diameter. The bottom of disk spins over the base of a thermo-foil heater. This thermo-foil heater is embedded inside a 40 mm thick balsa wood (thermal conductivity is about 0.06 W m^{-1} K^{-1} to minimize the heat loss from its back surface, supplying an approximately heat flux up to 5 kW m^{-2}. The electrical power for Joule heating is fed to heat foils through a transformer with the total power consumption metered by a wattmeter.

The temperature distributions on the top surface of disk are monitored by 13 thermocouples (T type, Copper-Constantan). These thermocouples are embedded in the disk with their junctions near the surface. They are arranged in a row along radial direction. All the thermocouple wires are taken out the disk via the grooves machined on the rotating disk back and then connected to the multi-channel slip ring unit rotating with the shaft. Besides, 5 thermocouples are used to measure the temperature on the back surface of insulator.

The real heating flux is determined as

$$q = \frac{Q}{A} = \frac{IE - Q_s}{A}, \tag{8}$$

where Q is the input power imposed on heating foil. I and E are electricity current and voltage imposed on the electrical heater. A is effective area of heating foil. Q_s is the heat loss from heater insulation, including radiation heat loss Q_r and nature convection heat loss Q_c.

$$Q_r = \varepsilon\sigma A(\overline{T}^4_{w,ins} - T_f^4), \tag{9}$$

where ε is the emissivity of the insulator, σ is a constant of black body radiation. $\overline{T}_{w,ins}$ is the temperature of insulator, T_f is the temperature of environment.

$$Q_c = h_z A(\overline{T}_{w,ins} - T_f), \tag{10}$$

where h_z is the convective heat transfer coefficient between insulator and environment, which is determined by the empirical relations for natural convection heat transfer [30].

Figure 6 presents the computational results of flow field induced by rotating smooth disk at rotational speed of 2000 r min^{-1}. It is obviously viewed that the spiral fluid flow over a rotating disk is an extremely complicated three-dimensional motion. The predominant flow direction is tangential, but radial velocities across the disk are generated by centrifugal forces and this induces axial velocities toward the disk. The flow exhibits skewing of the velocity vector across the boundary layer. It is known that the skewing develops because a radial pressure gradient cannot be maintained in the infinite quiescent medium leaving nothing to oppose the centrifugal force felt by fluid elements. And the disk boundary layer is unique because it maintains nearly constant skewing all the way from its origin as a laminar boundary layer through its development as a turbulent boundary layer. As expected, the complicated flow over the rotating disk is reasonable for affecting the conjugate heat transfer of rotating disk.

Based on the heat flux distribution on the top of rotating disk, the local heat transfer coefficients are determined both from computation and from experiment, as shown in Figure 7. At relatively low rotational speed (such as 1000 r min^{-1}), the flow over the entire disk surface maintains laminar. The local heat transfer capacity is strong in the center of rotating disk where the surface is subjected to the impingement of pumping air jet. As the rotational speed increases, the entrainment of the ambient air toward the disk is enhanced to bring out a higher convective heat transfer coefficient at the center of the rotating disk. Simultaneously, the cyclone effect near the rotating disk surface is also enhanced, especially at the rim of the rotating disk, which results in heat transfer enhancement. By comparison, it is shown that the computational results are consistent with the experiment data.

4 Thermal transport inside rotating porous disk

Figure 8 presents the flow fields inside porous disk at rotational speed of 0 and 1000 r min^{-1}, with porosity of 0.6.

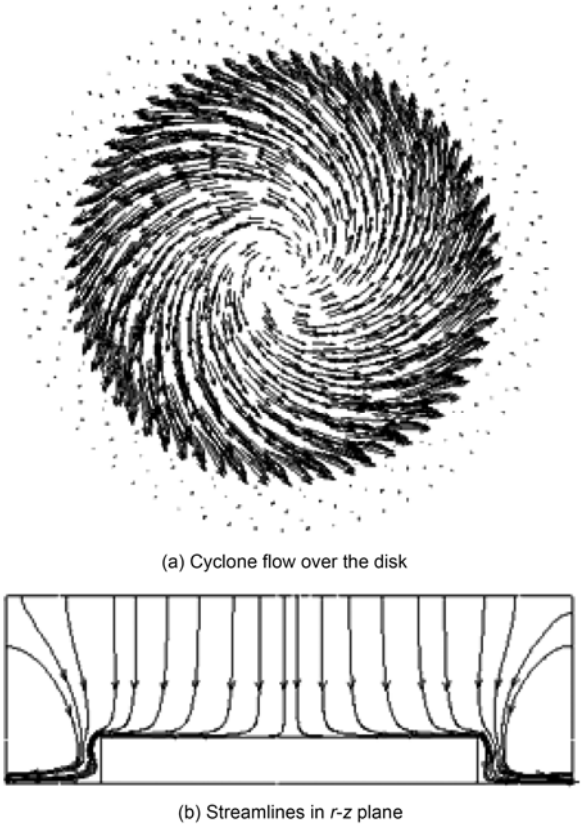

Figure 6 Flow fields induced by rotating disk.

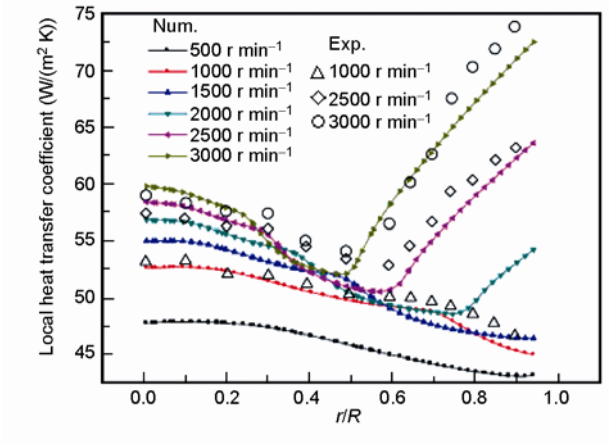

Figure 7 Radial distribution of convective heat transfer coefficient on rotating smooth disk.

When the porous disk is in still status, the fluid near the heating zone flows upwards under the gravitational force field, forming natural convection (as seen in Figure 8(a)). When the disk is driven to rotate, the thermally-driven natural convection under the centrifugal force field is enhanced obviously (as seen in Figure 8(b)). It is expected that this thermally-driven natural convection will couple with the azimuthal flow induced by the rotating disk.

Figure 9 presents the temperature distributions on the side surface of rotating disk under different rotational speeds. In these cases, the porosity and material of the solid matrix are set as 0.6 and pure aluminum (conductivity is regarded as 200 W m^{-1} K^{-1}, respectively. When the disk rotates at 500 r min^{-1}, the temperature in the vicinity of heating zone is high with respect to the rotational direction. Simultaneously, high temperature gradient also occurs in this heating zone. As the rotational speed increases, the centrifugally-driven thermal convection is enhanced, and the heat transfer capacity from the disk to the surrounding ambient is also enhanced, leading to the decrease of local temperature in the vicinity of heating zone and the homogenization of the temperature over the disk surface. It is observed that the isotherm lines tend to be circular once the rotational speed reaches up to 1500 r min^{-1}.

Figure 10 presents the temperature distributions on the rim surface of rotating disk under different rotational speeds. The apparition of a thermal trail is observed at the downstream of the heated region, especially under high rotational speed. This behavior is similar to the heat conduction on a two-dimensional plate subjected to the moving heat source.

Figure 11 illustrates the effect of the rotational speed on the highest temperature and maximum temperature difference on the disk. Here the maximum temperature difference represents the difference between the highest temperature and the lowest temperature on the disk. When the rotational speed increases from 500 to 1500 r min^{-1}, the highest temperature on the disk is decreased by about 13.2 K. When the disk rotates at 500 r min^{-1}, the maximum temperature difference on the disk is about 25.2 K. When the disk rotates at 750 r min^{-1}, the maximum temperature difference is about 16.9 K. When the disk rotates at 1500 r min^{-1}, the maximum temperature difference is about 10.2 K. This is an indication of stronger conjugation of centrifugally-driven thermal convection inside porous disk and swirl convection over the disk surface under higher rotational speed.

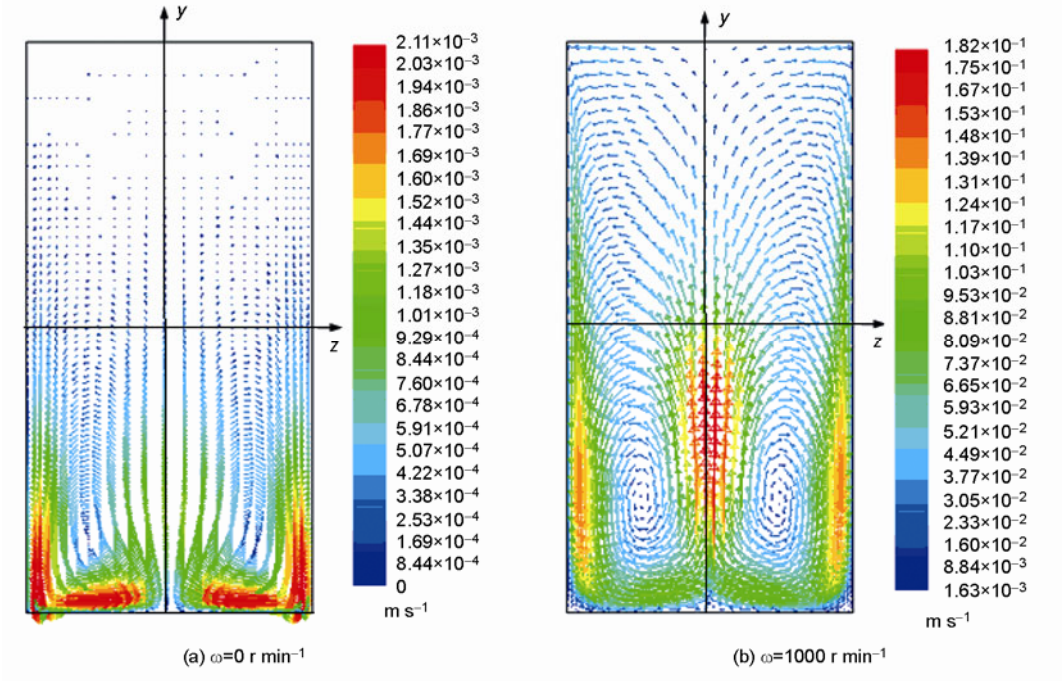

Figure 8 Thermally-driven natural flow fields inside porous disk.

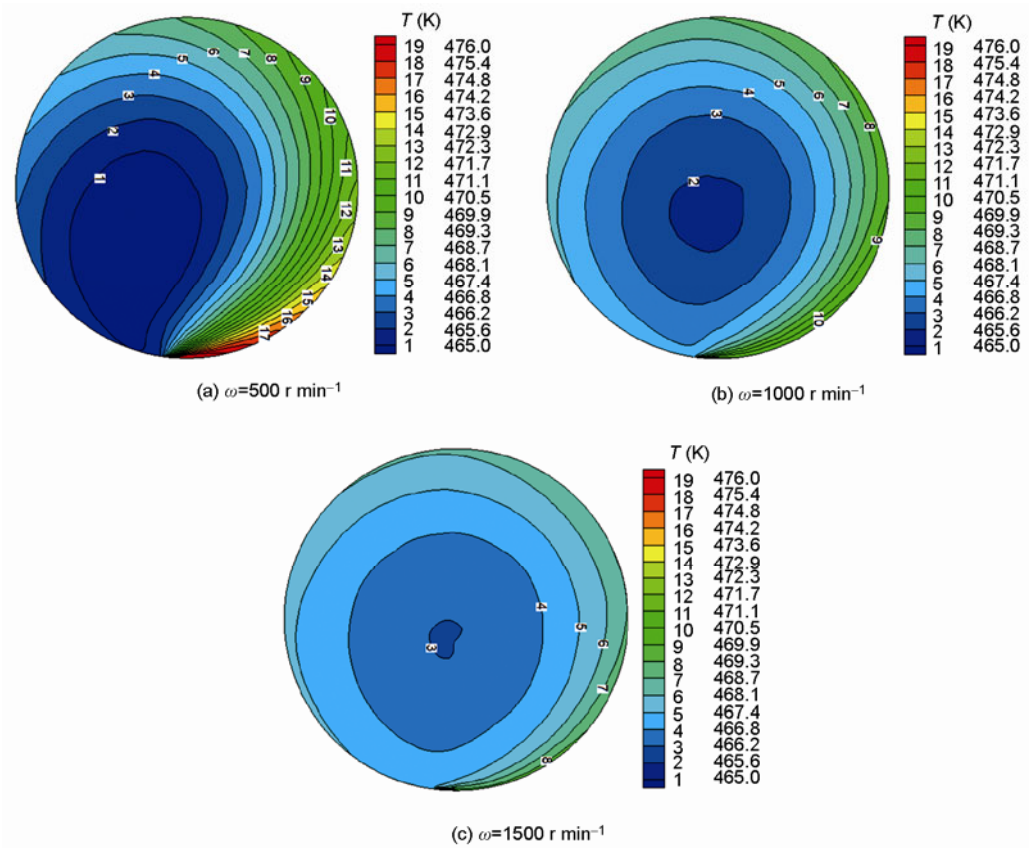

Figure 9 Temperature distribution on rotating disk surface.

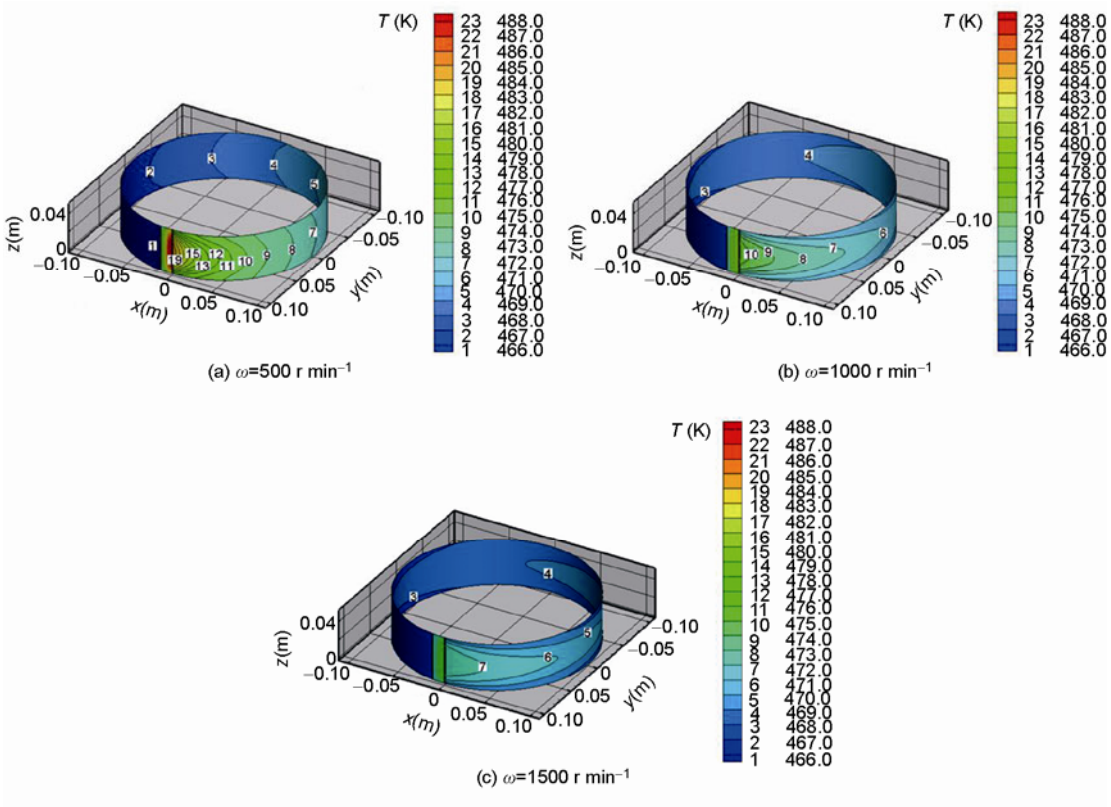

Figure 10 Temperature distribution on rotating disk rim.

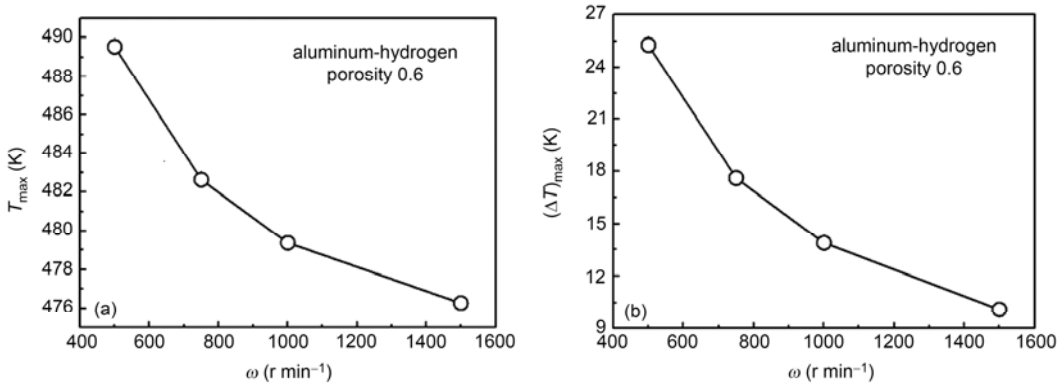

Figure 11 Effect of rotational speed on temperature distributions. (a) Highest temperature; (b) maximum temperature difference.

To evaluate the thermal transport capacity inside rotating porous disk, a performance parameter named thermal transport coefficient is introduced in the present, similar to the definition of convective heat transfer coefficient

$$E = \frac{q}{T_{\max} - T_{\min}}, \tag{11}$$

where q is local heat flux on the sectional arc located at the disk rim, $T_{\max}$ and $T_{\min}$ are the highest temperature and the lowest temperature on the disk, respectively.

When the disk rotates at 500 r min^{-1}, the thermal transport coefficient is about 1.98×10^4 W m^{-2} K^{-1}. When the disk rotates at 1000 r min^{-1}, the thermal transport coefficient is about 3.62×10^4 W m^{-2} K^{-1}, with approximate 83% enhancement in comparison with that of 500 r min^{-1}. When the disk rotates at 1500 r min^{-1}, the thermal transport coefficient is about 4.9×10^4 W m^{-2} K^{-1}, with approximate 148% enhancement in comparison with that of 500 r min^{-1}. The stronger the thermal transport capacity in rotating porous disk is, the more uniform the temperature distribution displays.

5 Effects of porosity and conductivity of solid matrix

Figure 12 illustrates the effect of the conductivity of solid matrix on the highest temperature and maximum temperature difference on the disk. In these cases, the porosity of the solid matrix is set as 0.8 and the rotational speed is set as 1000 r min^{-1}. Four representative combinations of high porosity matrix and fluid are considered in the present work. They are stainless steel-hydrogen (solid matrix conductivity is regarded as 17 W m^{-1} K^{-1}, pure nickel-hydrogen (solid matrix conductivity is regarded as 85 W m^{-1} K^{-1}, aluminum-hydrogen (solid matrix conductivity is regarded as 200 W m^{-1} K^{-1}, and pure copper-hydrogen (solid matrix conductivity is regarded as 385 W m^{-1} K^{-1}, respectively. According to the definition of effective conductivity of porous medium (eq. (5)), the corresponding effective thermal conductivities are 0.36, 17.2, 40.2 and 77.2 W m^{-1} K^{-1}, in turn.

For the stainless steel-hydrogen combination, the highest temperature is about 490.5 K and the maximum temperature difference on the disk is about 24.8 K, the corresponding thermal transport coefficient is about 2.02×10^4 W m^{-2} K^{-1}. While for the pure copper-hydrogen combination, the highest temperature is about 478 K and the maximum temperature difference on the disk is about 12.8 K, the corresponding thermal transport coefficient is about 3.9×10^4 W m^{-2} K^{-1}. The heat transfer performance is improved for copper-hydrogen combination due to high solid thermal conductivity of metallic foams. In this case, the relative dominance of conduction heat transfer to convection heat transfer inside porous medium is great.

The effect of the porosity of solid matrix on the highest temperature and maximum temperature difference on the disk is reported in Figure 13. In these cases, the material of the solid matrix is set as pure aluminum and the rotational speed is set as 1000 r min^{-1}. The porosity of solid matrix is varied from 0.4 to 0.8.

It is observed that both the highest temperature and the maximum temperature difference on the disk are decreased with the decrease of the solid matrix porosity. As porosity decreases, the interfacial surface area and associated effective thermal conductivity increase, contributing to heat conduction enhancement inside porous disk. But on the other hand, it is noticed that both the highest temperature and the maximum temperature difference on the disk are decreased weakly when the porosity increases from 0.4 to 0.8. This behavior may be associated with the damping effect of the porosity on the flow capacity inside rotating porous disk, as seen in Figure 14. The centrifugally-driven flow is weakened as the decrease of porosity, leading to less thermal transport by the convection mode. Taking the porosity of 0.6 as an example, the effective thermal conductivity for aluminum-hydrogen combination is 80.1 W m^{-1} K^{-1}. In this case, the highest temperature and the maximum

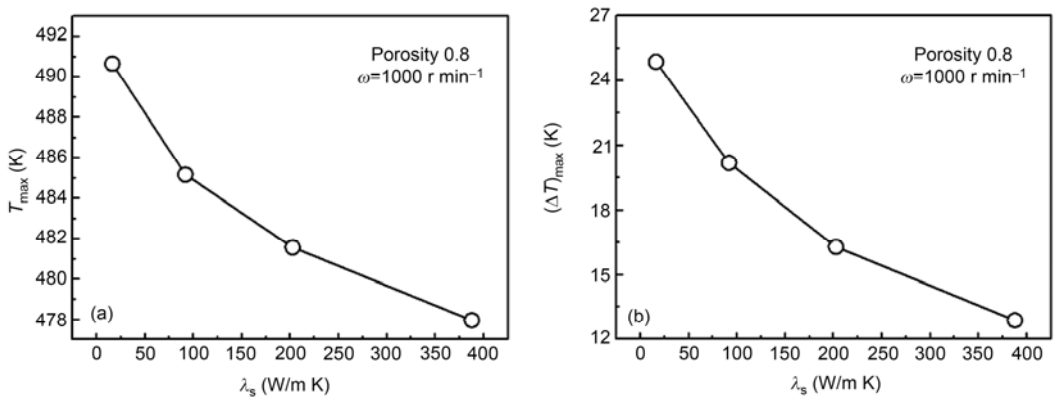

Figure 12 Effect of solid thermal conductivity on temperature distributions. (a) Highest temperature; (b) maximum temperature difference.

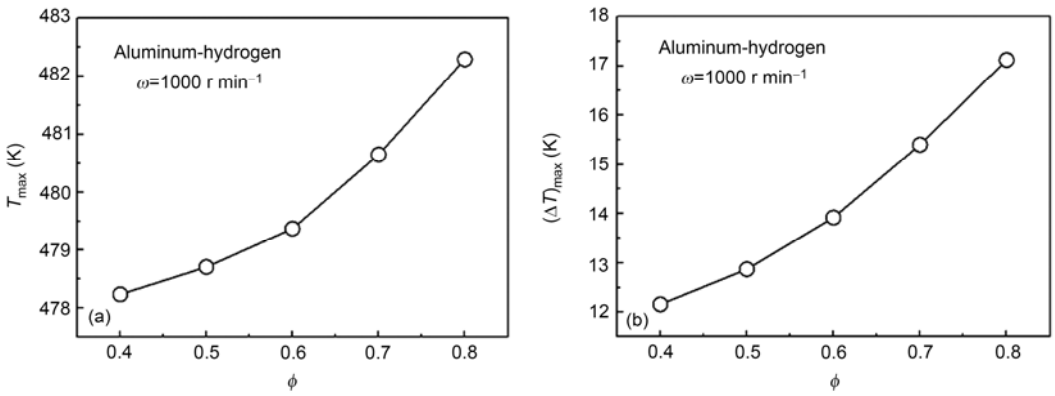

Figure 13 Effect of solid porosity on temperature distributions. (a) Highest temperature; (b) maximum temperature difference.

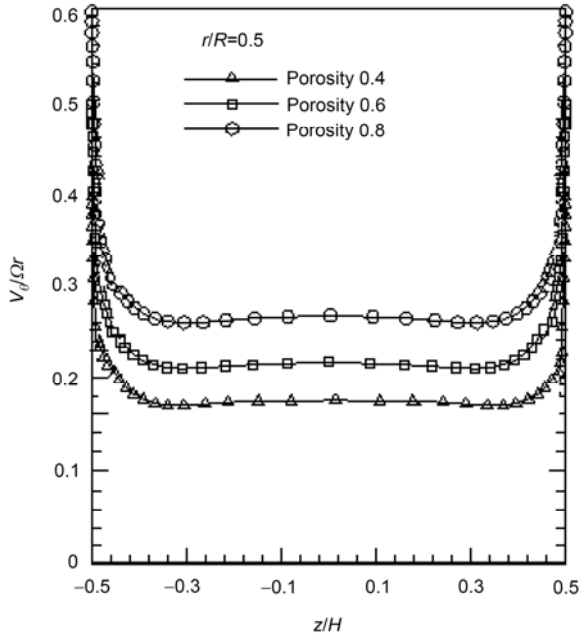

Figure 14 Effect of solid porosity on azimuthal velocity distributions inside porous disk.

temperature difference on the disk are 479.4 and 13.8 K, respectively. They are little higher than those values corresponding to copper-hydrogen combination with porosity of 0.8 (as seen in Figure 13), while the latter case has the effective thermal conductivity of 77.2 W m^{-1} K^{-1}.

For the aluminum-hydrogen combination and fixed rotational speed of 1000 r min^{-1}, when the porosity is 0.4, the thermal transport coefficient is about 4.15×10^4 W m^{-2} K^{-1}. When the porosity is 0.6, the thermal transport coefficient is about 3.62×10^4 W m^{-2} K^{-1}, with approximate 12.8% decrease in comparison with that of 0.4. When the porosity is 0.8, the thermal transport coefficient is about 2.93×10^4 W m^{-2} K^{-1}, with approximate 29.4% decrease in comparison with that of 0.4.

In the rotating porous disk, the solid phase heat transfer is clearly the dominant mode of heat transport and the fluid phase makes an incremental contribution to the total heat transfer.

6 Conclusions

1) As the rotational speed of disk increases, the centrifu-

gally-driven thermal convection is enhanced, and the heat transfer capacity from the disk to the surrounding ambient is also enhanced, leading to the decrease of local temperature in the vicinity of heating zone and the homogenization of the temperature over the disk surface.

2) The thermal transport capacity in rotating porous disk is enhanced with the increase of solid thermal conductivity or the decrease of solid porosity. In the rotating porous disk, the solid phase heat transfer is clearly the dominant mode of heat transport and the fluid phase makes an incremental contribution to the total heat transfer.

3) For the aluminum-hydrogen combination, the thermal transport coefficient is enhanced approximately 150% when the rotational speed increases from 500 to 1500 r min^{-1}, and the thermal transport coefficient is decreased by approximately 30% when the porosity increases from 0.4 to 0.8. The thermal transport coefficient for the pure copper-hydrogen combination is nearly twice that of stainless steel-hydrogen combination.

This work was supported by the National Natural Science Foundation of China (Grant No. 51076063).

1 Ramesh K, Huang H, Yin L. Analytical and experimental investigation of coolant velocity in high speed grinding. Int J Mach Tool Manu, 2004, 44: 1069−1076
2 Kovacevic R, Cherukuthota C, Mazurkiewicz M. High pressure water jet cooling/lubrication to improve machining efficiency in milling. Int J Mach Tool Manu, 1995, 35: 1459−1473
3 Xiao B, Xu H J, Fu Y C, et al. Study on grinding burn with radial water jet impingement cooling and brazed grinding wheel (in Chinese). Chinese J Mech Eng, 2002, 38(1): 91−94
4 Kaminski J, Alvelid B. Temperature reduction in the cutting zone in water-jet assisted turning. J Mater Proc Technol, 2000, 106: 68−73
5 Xu H J, Fu Y C, Sun F H, et al. Fundamental studies on enhancing heat transfer in contact zone during high efficiency grinding. Sci China Ser E-Tech Sci, 2002, 45(3): 261−272
6 Babic D, Murray D B, Torrance A A. Mist jet cooling of grinding processes. Int J Mach Tool Manu, 2005, 45: 1171−1177
7 Liu J Y, Han R D, Sun Y F. Research on experiments and action mechanism with water vapor as coolant and lubricant in green cutting. Int J Mach Tool Manu, 2005, 45(6): 687−694
8 An Q L, Fu Y C, Xu J H, et al. The application of cryogenic pneumatic mist jet impinging in high-speed milling of Ti-6Al-4V. Key Eng Mater, 2006, 315-316: 244−248
9 Zhang J Z, Tan X M, Liu B, et al. Investigation for convective heat transfer on grinding work-piece surface subjected to a mist/air impinging jet. Appl Therm Eng, 2013, 51: 653−661
10 Su H H, Ma K, Fu Y C, et al. Investigation of enhancing heat transfer in grinding zone with loop heat pipe wheel. J Nanjing Univ Aeronaut Astronaut, 2012, 44(2): 233−239
11 Wang S, Guo Z Y, Li Z X. Heat transfer enhancement by using metallic filament insert in channel flow. Int J Heat Mass Transfer, 2001, 44: 1373−1378
12 Pavel B I, Mohamad A A. An experimental and numerical study on heat transfer enhancement for gas heat exchangers fitted with porou media. Int J Heat Mass Transfer, 2004, 47: 4939−4952
13 Zhao C Y, Kim T, Lu T J, et al. Thermal transport in high porosity cellular metal foams. J Thermophys Heat Transfer, 2004, 18: 309−317
14 Tzeng S C, Soong C Y, Wong S C. Heat transfer in rotating channel with open cell porous aluminum foam. Int Commu Heat Mass Transfer, 2004, 31(2): 344−348
15 Braga E J, DeLemos M J S. Computation of turbulent free convection in left and right tilted porous enclosures using a macroscopic k-ε model. Int J Heat Mass Transfer, 2008, 51: 5279−5287
16 Zhao P H, Ye T H, Zhu M M, et al. Numerical investigation on hydrogen production by CH4-Rich combustion in an alumina foam. Sci China Tech Sci, 2009, 52(10): 2960−2966
17 Zhao K, Li Q, Xuan Y M. Investigation on the three-dimensional multiphase conjugate conduction problem inside porous wick with the lattice Boltzmann method. Sci China Tech Sci, 2009, 52(10): 2973− 2980
18 Jiang P X, Xiang H, Xu R N. Theoretical and experimental study of the thermal conductivity of nanoporous media. Sci China Tech Sci, 2012, 55(8): 2140−2147
19 Chen C C, Huang P C, Hwang H Y. Enhanced forced convective cooling of heat sources by metal-foam porous layers. Int J Heat Mass Transfer, 2013, 58: 356−373
20 Jou J J, Liaw J S. Thermal convection in a porous medium subject to transient heating and rotation. Int J Heat Mass Transfer, 1987, 30: 208−211
21 Vadasz P. Convection and stability in a rotating porous layer with alternating direction of the centrifugal body force. Int J Heat Mass Transfer, 1996, 39: 1639−1647
22 Alex S M, Patil P R. Thermal instability in an anisotropic rotating porous medium. J Fluid Mech, 2000, 252: 79−98
23 Beg O A, Takhar H S, Beg T A, et al. Modelling convection heat transfer in a rotating fluid in a thermally-stratified high-porosity medium: numerical finite difference solutions. Int J Fluid Mech Res, 2005, 32: 383−401
24 Xia J, Chang H P. Effect of different porosity on thermally driven heat transfer in a centrifugal force field (in Chinese). J Aerosp Power, 2006, 21(6): 972−977
25 Lee D Y, Vafai K. Analytical characterization and conceptual assessment of solid and fluid temperature differentials in porous media. Int J Heat Mass Transfer, 1999, 42: 423−435
26 Alazmi B, Vafai K. Analysis of fluid flow and heat transfer interfacial conditions between a porous medium and a fluid layer. Int J Heat Mass Transfer, 2001, 44: 1735−1749
27 Kim S J, Jang S P. Effects of the Darcy number, the Prandtl number and the Reynolds number on the local thermal non-equilibrium. Int J Heat Mass Transfer, 2002, 45: 3885−3896
28 Nield D A. Modelling fluid flow and heat transfer in a saturated porous medium. J Appl Math Decis Sci, 2000, 4: 165−173
29 ANSYS Fluent v12.0 Software User's Gide, 2009
30 Holman J P. Heat Transfer. 9th ed. New York: McGraw-Hill, 2002